Volumetric Fingerprint Data Analysis using Optical Coherence Tomography

Ctirad Sousedik[1], Ralph Breithaupt[2], Christoph Busch[1]

[1]Norwegian Biometrics Laboratory
Gjøvik University College
Teknologiveien 22
2815 Gjøvik, Norway
ctirad.sousedik@hig.no
christoph.busch@hig.no

[2]Federal Office for Information Security
53133 Bonn, Germany
ralph.breithaupt@bsi.bund.de

Abstract: The increasing usage of fingerprint biometrics as a security technology requires the biometric systems to be resistant against moderate or even high attack potential. To date, state-of-the-art fingerprint sensors can be deceived by using an accurate imitation of the ridge/valley pattern of an enrolled fingerprint that can be produced utilizing low-cost, commonly available materials and techniques. The structure of high-resolution 3D volumetric scans of fingertips, acquired by using the Optical Coherence Tomography (OCT), has been analyzed by this work so that a Presentation Attack Detection method could be developed that would render the artefact production process extremely difficult or even practically impossible.

1 Introduction

The fingerprint biometrics is increasingly being applied as a means of access control to security sensitive facilities or sensitive data. The economic constraints further motivate cost saving decisions and thus unsupervised operation of fingerprint based access control has been considered. Recently, the wide availability of the fingerprint sensors on the market has enabled their application also to rather common purposes or facilities such as recreation areas, fitness centers, etc.

The increasing usage of fingerprint biometrics as a security technology requires the biometric systems to be resistant against moderate or even high attack potential [Mun12]. The fingerprint biometrics, as well as any other biometric mode, can be deceived by an accurate artificial representation of the original characteristic and spoofing of fingerprint systems, as well as the development of efficient countermeasures, is one of the most relevant research areas at present. The majority of the state-of-the-art fingerprint sensors can be deceived by an accurate imitation of the fingerprint created by using low-cost and widely available materials and techniques [GFAFMD11].

Numerous approaches to solve the problem of fingerprint liveness detection have been suggested in literature [SMB10]. In order to avoid the costs related to an update of the

sensing technology hardware, researchers and manufacturers attempted to develop liveness detection methods that make use of the 2D fingerprint representations provided by the classical sensors. The methods analyze patterns in the 2D scans that occur due to differences between the genuine fingers and their artificial counterparts, such as inaccurate reproduction of a genuine finger, different elasticity of the artefact material, absence of the skin perspiration etc. However, the limited performance of the state-of-the-art 2D based liveness detection methods rather points to the fact that 2D scans might not be sufficient to be able to distinguish between genuine and artefact or cut-off fingers [YGD+12].

Another group of approaches suggest an update of the hardware parts of the sensing technology by using supplementary sensors that would provide for additional information usable for the liveness detection. Due to large variety of possible artefact material and production techniques, a single aspect dedicated liveness detection sensor can usually be deceived if an appropriate new combination of materials and techniques has been proposed. In order to increase the difficulty of producing an artefact, some manufacturers try to include a larger number of such supplementary sensors that would capture information about multiple aspects of the scanned characteristic. This approach requires application of machine learning techniques to process information from all sensors and take the final decision whether a genuine characteristic has been presented. Since performance of a machine learning based classifier depends on the training data, the sensor can still be vulnerable if an entirely new material and production technique has been used to produce the artefact characteristic.

The above mentioned challenges have motivated a search for a single sensing technology that would provide for a sufficiently detailed representation of the biometric characteristic and could be used both for the presentation attack detection[ISO], as well as biometric recognition. This paper proposes a method for analyzing the structure of fingerprint scans provided by the Optical Coherence Tomography (OCT). The OCT allows to obtain a 3D volumetric representation of the scanned fingerprint, capturing not only the outer fingerprint but also the inner skin structures up to depth of 2-3 mm. Specifically we are interested in the boundary between the inner dermis and the outer epidermis, which contains the *master-template* of the fingerprint pattern. This *inner* fingerprint is responsible for regeneration and stability of the outer fingerprint pattern and it can be captured and visualized by the OCT. Small internal structures, such as sweat glands, are also represented in an OCT scan and can be used for liveness detection purposes. A reliable automated liveness detection analysis of an OCT scan would render the production of an appropriate fake representation (i.e. artifact) extremely difficult or even impossible in practice.

2 Optical Coherence Tomography for Fingerprints

The Optical Coherence Tomography is a 3D scanning technology that has originally been developed for medical purposes. It is capable of capturing volumetric representations of the scanned object up to depth of 2-3mm under the surface and the captured signal is a function of the scattering properties of the material. In the classical Time-Domain OCT (TD-OCT) design, a beam of light of low coherence length and wavelength of about 830nm

is split into two separate beams. The first beam is targeted at the object and reflects back. The second beam is targeted by means of a reference arm in such manner that it interferes with the beam reflected from the object. Due to low coherence length of the light source, the interference takes place only with the light reflected from a certain depth under the object surface and the amount of the light reflected can be measured [CSF06].

The classical TD-OCT design requires the reference arm to be positioned in all three axes x, y, z, in order to capture a single voxel, which makes it rather slow, if a full volumetric representation is to be acquired. The OCT based scanning devices exist in multiple adaptations of the original design, in order to achieve higher scanning speeds. Full-Field OCT (FF-OCT) makes use of a 2D array of detectors that can capture the entire (x, y) slice in a single measurement. The Fourier-Domain OCT (FD-OCT) and Swept-Source OCT (SS-OCT) utilize the properties of Fourier Transform to acquire full depth scans without movement of the reference arm along the axis, z [CSF06].

The potential of the OCT technology for the fingerprint presentation attack detection scenario was researched by the project *OCT-Finger* [OCT10]. The test group individuals were able to achieve almost 100% manual recognition rate on a large-scale database of OCT scans of genuine and artefact fingerprints. The study has demonstrated that, apart of the outer fingerprint pattern, the OCT technology has also the potential to capture the structure of the inner fingerprint tissues that are responsible for stability and regeneration of the outer fingerprint, as well as small internal skin structures such as sweat glands (Fig. 1).

The project has demonstrated that the OCT technology allows for analysis of multiple aspects that differentiate genuine and artefact fingers. The 3D representation of the outer fingerprint provides for more information than a classical 2D fingerprint scan. The sweat glands underneath could be detected and their helix-like structure, as well as other properties, verified. In genuine scans, the inner fingerprint pattern copies the pattern of the outer fingerprint and therefore successful comparison of the two patterns could provide for a strong evidence of a genuine finger scan. Other possibilities include verification of the scattering properties of the fingertip skin that potentially differs from the scattering properties of an artefact material. It can be assumed that replication of the internal structure and the scattering properties represented in an OCT scan by means of an artefact would be extremely difficult.

Nevertheless, an efficient liveness detection method based on volumetric scans of fingertips has to cope with a number of challenges. A volumetric OCT scan represents a significant amount of data that increases very quickly with its resolution. A scan of resolution $200 \times 200 \times 512$ voxels ($width \times height \times depth$) represents 19,5 MB of data and a scan of $1024 \times 1024 \times 512$ voxels 512 MB of data if a voxel is represented by a single byte. The acquisition time typically increases with the scanning resolution, which limits practically achievable resolutions. For practical applicability, all the data need to be captured and processed in a matter of a few seconds. As depends on the quality of the OCT scanner and the scattering properties of the fingertip skin, the resulting scan is subject to some amount of speckle noise along with a number of faulty measurements. The structure of the noise can vary slightly among the scanning devices, and the method should deal with the noise in device-independent fashion. The intra-class variability of properties of

genuine human fingers is relatively large and an efficient classification method has to be able to reliably distinguish between the genuine structures and the structures achievable in artefact fingers. In order to reliably classify previously unknown artefacts, the method should validate properties of genuine fingers rather than try to detect anomalies caused by artefact fingers.

Based on the data collected in the framework of the *OCT-Finger* project, Menrath and Breithaupt [Men11] have proposed an automatic method for analysis and classification of the OCT scans into genuine and artefact ones. They preprocess the OCT volumetric scans by using 3D median filters to suppress the influence of the speckle noise and faulty measurements in the analysed data. The filtered volume is then searched for the inner and outer fingerprint and sweat glands are attempted to be extracted. Due to 3D filtering of a large amount of data, the approach turned out to be an order of magnitude slower than required for practical application. Even though an attempt to perform massive parallelization of their method successfully resulted in a speed-up of an order of a magnitude, the method remains very computationally intensive, which limits its applicability to scans of larger resolutions.

3 Fingerprint Skin Layer Separation

3.1 Database

The OCT scan database used in this work has been composed within the framework of the *OCT-Finger* [OCT10]. The OCT scanning device was based on the Fourier-Domain OCT (FD-OCT) technology with an acquisition time of $2.24s$ per scan and operating on a wavelength of $1300 \pm 55nm$. A scan represents $4 \times 4 \times 2.5mm$-large volume ($width \times height \times depth$) of the fingertip at a resolution of $200 \times 200 \times 512$ voxels.

The scans of genuine living fingers represent fingers of 226 subjects of which 96 (42%) were males and 130 (58%) females. The age structure has been as follows: 18 subjects (8%), 5-20 years; 172 subjects (76%), 20-60 years; 36 subjects (16%), 60-80 years. For each subject, at least the right thumb, the right index finger and the right little finger was scanned. Each finger instance was scanned 11 times, which provided for the minimum total amount of 7458 samples of genuine living finger scans.

The fake fingerprint scans represent 30 different classes of artefact fingerprints. The variation artefacts is caused by the mold material composition (gelatin, silicone, latex, window paint, wood glue etc.) and the artefact material composition (glycerol, graphite, window paint etc.). For each class, at least 9 artefact fingerprints were produced. Each of the artefact fingerprints was used to acquire at least 11 scans, yielding for minimum number of 2970 artefact fingerprint scans.

In addition to that, fingers of 5 male and 5 female dead bodies were scanned. For each body, 3 fingers were scanned, 11 times each, providing for 330 dead finger samples.

3.2 Scan Structure

As illustrated by Fig. 1, the OCT technology is able to capture the layered structure of the skin of human fingers. The scan captures a strong reflection from the boundary between the air and the outer fingerprint (Fig. 1b). The outer fingerprint layer is followed by a layer containing the sweat glands. Thickness of this layer as well as its scattering properties vary in the skin of different subjects. The amount of sweat glands also varies strongly among subjects. Some subjects can provide ten times more sweat glands than other subjects and for some individuals the OCT scan is completely lacking any sweat glands. The layer containing sweat glands is followed by a layer that contains the inner fingerprint. The inner fingerprint (i.e. dermis boundary) is a cell structure responsible for stability and regeneration of the outer fingerprint. Unless the inner fingerprint is damaged, the outer fingerprint can fully regenerate to the original pattern. The structure of the outer fingerprint is typically a copy of the inner fingerprint (however, the thickness, clarity and strength of its reflection widely varies among subjects).

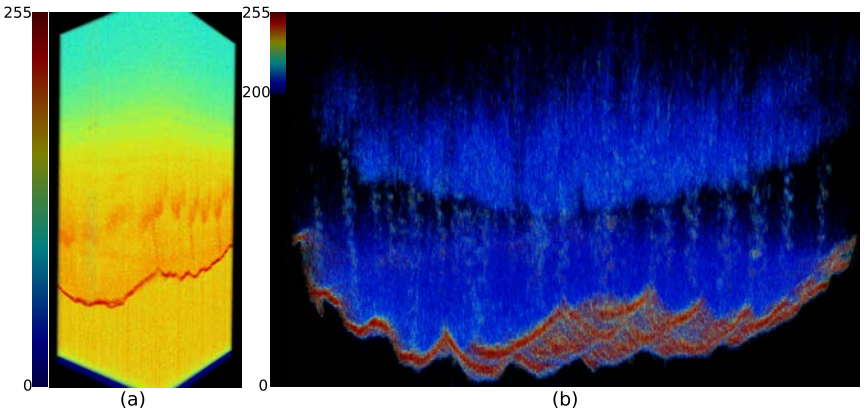

Figure 1: (a) OCT scan of a genuine finger (b) OCT scan of a genuine finger, thresholded 200+, heat-map scale change allows for clearer visualization of fine structures such as sweat glands

A typical structure of a scan of an artefact fingerprint differs in various aspects (Fig. 2) from the genuine counter piece. A thin layered artefact typically yields a strong reflection layer from its outer surface. The structure of the next layer depends on scattering properties and inner structure of the artefact fingerprint (Fig. 2a). Unless the artefact fingerprint is too thick or impenetrable for the OCT scanner, a second strong reflection of the boundary between the artefact and the genuine fingerprint appears. The following structure then copies the genuine fingerprint structure. If the artefact fingerprint is too thick or its material too difficult to penetrate for the OCT scanner, only an outer fingerprint reflection appears (Fig. 2b). The following layer of data represents scattering properties and inner structure of the artefact material (bubbles etc.). A second layer of the inner fingerprint does not appear, nor does it copy the pattern of the outer fingerprint.

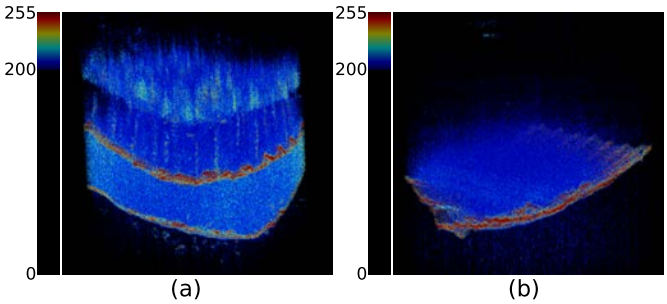

Figure 2: (a) OCT scan of a thin-layered artefact on a genuine finger (b) OCT scan of a thick artefact fingerprint

3.3 Automatic Method

In order to cope with the large amount of volumetric data in an OCT scan, the initial detection of positions of the specific layers in an OCT fingerprint scan should ideally avoid computationally expensive preprocessing of the data by 3D filtering. We propose a layer detection method robust to a certain degree of speckle noise and faulty measurements that can perform the initial layer detection directly. The volumetric scan, $V(x, y, z)$, of size, $w \times h \times d$, is analyzed as follows. A grid of size w_g and h_g is positioned over the (x, y) plane of the volume $V(x, y, z)$ (Fig. 3). Each grid cell yields a column volume, $C_{m,n}(x, y, z)$. From each of the columns, $C_{m,n}(x, y, z)$, a column accumulation function, $f_{m,n}(z)$, is computed as follows (Fig. 3):

$$f_{m,n}(z) = \sum_{x=0}^{\lfloor w/w_g \rfloor - 1} \sum_{y=0}^{\lfloor h/h_g \rfloor - 1} C_{m,n}(x, y, z) \tag{1}$$

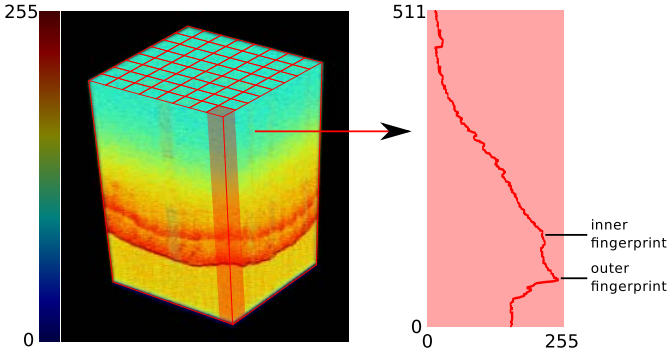

Figure 3: Extraction of the accumulation functions by means of a grid

For genuine living fingers, the shape of the column accumulation function $f_{m,n}(z)$ typically contains two intuitively observable peaks, one for the outer fingerprint and one for the inner fingerprint layer (Fig. 3). However, the two peaks are not always associated with the two main *global* maxima of the function. Due to noise in the volumetric data, one peak typically consists of multiple smaller peaks, while the actual center of the layer lies in the center of mass of the smaller peaks, rather than on one of them. A particular peak width range should be taken into consideration while searching for the peaks. In addition, the peaks themselves do not often form a maximum even in a smaller window of the function. They rather represent a sudden change on the shape of a function with an otherwise constantly growing or decreasing trend, typically a peak-like fluctuation that does not represent a maximum. Therefore, the peak localization method should look for the fluctuations taking the width range of the peaks into consideration and it should not be affected by the general slope of the function $f_{m,n}(z)$.

For an otherwise constant discrete function, $f(n)$, defined on interval, $[0, l-1]$, where l is a peak width parameter, a position p and an energy e of a single peak on its shape can be detected as the phase and amplitude of function f_p as follows (Fig. 4):

$$sn(n) = \sin(\frac{1}{2}\frac{2\pi}{l} + n\frac{2\pi}{l}) \quad (2) \qquad cs(n) = \cos(\frac{1}{2}\frac{2\pi}{l} + n\frac{2\pi}{l}) \quad (3)$$

$$a = -\sum_{n=0}^{l-1} f(n)sn(n) \quad (4) \qquad b = -\sum_{n=0}^{l-1} f(n)cs(n) \quad (5)$$

$$f_p = a \cdot sn(n) + b \cdot cs(n) \quad (6) \qquad e = \sqrt{a^2 + b^2} \quad (7)$$

$$p = \begin{cases} \frac{atan2(a,b)}{pi}\frac{1}{2}l & atan2(a,b) \geq 0 \\ l + \frac{atan2(a,b)}{pi}\frac{1}{2}l & atan2(a,b) < 0 \end{cases} \quad (8)$$

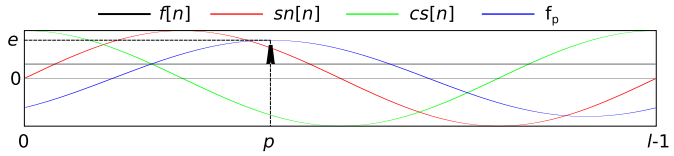

Figure 4: Peak detection for an otherwise constant function

However, if the discrete function, apart from the peak range, exhibits a constantly increasing or decreasing trend, the above mentioned method fails. Instead of pointing to the peak position, the method rather analyzes the strength of the global slope of the function $f(n)$. For an otherwise constantly increasing or decreasing function $g(n)$ defined on interval $[0, N-1]$ and $N = \frac{3}{2}l$, the following method can be used to detect a peak of energy e and position, p, as the phase and amplitude of function f_p (Fig. 5):

$$sn(n) = \sin(\frac{1}{2}\frac{2\pi}{l} + n\frac{2\pi}{l}) \quad (9) \qquad cs(n) = \cos(\frac{1}{2}\frac{2\pi}{l} + n\frac{2\pi}{l}) \quad (10)$$

$$a = \sum_{n=0}^{l-1} g(n)sn(n) \quad (11) \qquad b = \sum_{n=0}^{l-1} g(n)cs(n) \quad (12)$$

$$c = \sum_{n=0}^{l-1} g(n + \frac{1}{3}N)sn(n) \quad (13) \qquad d = \sum_{n=0}^{l-1} g(n + \frac{1}{3}N)cs(n) \quad (14)$$

$$f_p = (c-a)sn(n - \frac{1}{3}N) + (d-b)cs(n - \frac{1}{3}N) \quad (15)$$

$$e = \sqrt{(c-a)^2 + (d-b)^2} \quad (16)$$

$$p = \begin{cases} \frac{atan2(c-a,d-b)}{pi}\frac{1}{2}l + \frac{1}{2}l & atan2(c-a, d-b) \geq 0 \\ l + \frac{atan2(c-a,d-b)}{pi}\frac{1}{2}l + \frac{1}{2}l & atan2(c-a, d-b) < 0 \end{cases} \quad (17)$$

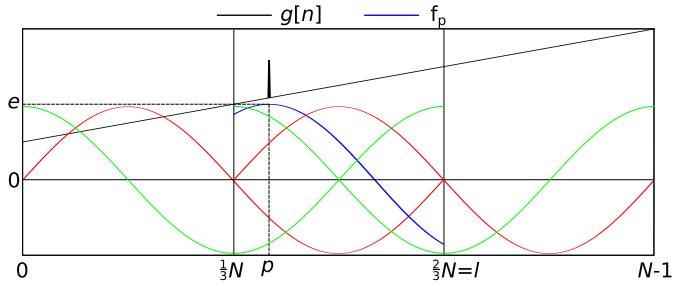

Figure 5: Peak detection an otherwise constantly increasing or decreasing function

The actual detection of positive fluctuations on the shape of a column accumulation function $f(n)$ defined on interval $[0, N_f - 1]$ is done by means of the following approach. The interval $[0, N_f - 1]$ is divided into overlapping windows $W_m = [m\frac{1}{4}l, m\frac{1}{4}l + \frac{3}{2}l - 1]$, where $m \geq 0$ (Fig. 6). For each window W_m the peak position p_m and energy e_m is computed using equations (9)-(17). Since $\sin(\alpha + \frac{\pi}{2}) = \cos(\alpha)$ and $\cos(\alpha + \frac{\pi}{2}) = -\sin(\alpha)$, the following set of equations can be used to efficiently compute a_m, b_m, c_m, d_m (eq. (11)-(14)) for a window W_m:

$$sns(o) = \sum_{n=o\cdot l/4}^{o\cdot l/4+l/4-1} f(n)\sin(\frac{1}{2}\frac{2\pi}{l} + n\frac{2\pi}{l}) \quad (18)$$

$$css(o) = \sum_{n=o\cdot l/4}^{o\cdot l/4+l/4-1} f(n)\cos(\frac{1}{2}\frac{2\pi}{l} + n\frac{2\pi}{l}) \quad (19)$$

if m is even:

$$a_m = \sum_{n=0}^{3} sns(m+n) \quad (20) \qquad b_m = \sum_{n=0}^{3} css(m+n) \quad (21)$$

$$c_m = \sum_{n=0}^{3} sns(m+n+2) \quad (22) \qquad d_m = \sum_{n=0}^{3} css(m+n+2) \quad (23)$$

if m is odd:

$$a_m = \sum_{n=0}^{3} -css(m+n) \quad (24) \qquad b_m = \sum_{n=0}^{3} sns(m+n) \quad (25)$$

$$c_m = \sum_{n=0}^{3} -css(m+n+2) \quad (26) \qquad d_m = \sum_{n=0}^{3} sns(m+n+2) \quad (27)$$

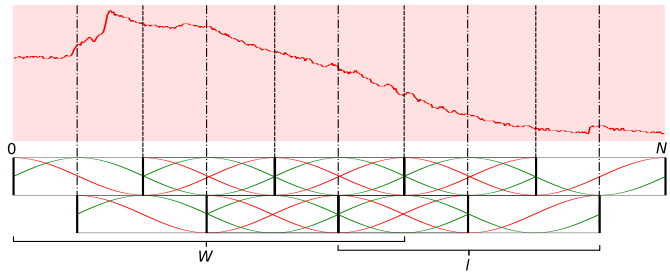

Figure 6: Overlapping windows for peak detection

Values of functions $sns(o)$ and $css(o)$ can be precomputed by a single multiplication of the analyzed function $f(n)$ with the function $sn(n)$ (eq. (9)), and the function, $cs(n)$ (eq. (10)), while storing the intermediate results. Each of the weights, a_m, b_m, c_m, d_m, can then be computed by adding 4 of these precomputed values. The method does not perform any convolution of any core function with the original function $f(n)$, which greatly reduces computational complexity as compared to a convolution based method. In addition the values of functions $sns(n)$ and $css(n)$ can be computed in parallel with no data overlap.

The windows W_m of length $\frac{3}{2}l$ are overlapping each other with an interval of $\frac{1}{4}l$. Consequently each of the windows W_m provides a reliable peak position p_m and peak energy e_m around its center in an interval of length, $\frac{1}{4}l$. If the detected peak position p falls outside of the central interval, it is discarded. The peaks that are detected inside of the central interval of their detection window W_m are considered in the further processing. Depending on the settings, P peaks ($P = 2$ for detection of two layers) with highest energy e are stored.

By means of the above described method P peaks are detected for each column accumu-

lation function $f_{m,n}(z)$ yielding for a sparse approximation of the position of the P most apparent layers in the scan volume $V(x, y, z)$.

4 Results

Manual inspection of the genuine fingerprint scans has identified about 11% of the scans as being of insufficient quality due to non-compliant behavior of the capture subjects. Clearly visible anomalies such as sudden missing parts of the scans and discontinuities in the structure of the scans are related to the fact that the finger was not held still during the scanning period, it was put too close to the scanning surface, removed before the scanning was finished, etc.

An example of the results of the method applied to genuine fingerprint scans ($P = 2$) is shown by Fig. 7. For the genuine fingerprint scans without the anomalies related to the non-compliant subject behavior, the method successfully detected the outer and inner fingerprint layer in 90% of the scans (less than 5% outliers, sparsely distributed) with an average processing time of 0.02s in a single thread on a 3.6GHz 64bit CPU, as opposed to 56s in a single thread on a 2.5GHz CPU as reported by Menrath and Breithaupt [Men11]. The unsuccessful cases were caused by a very weak or completely missing representation of an inner fingerprint in the OCT scan. If the inner fingerprint was present to some extent, the method still did succeed to represent its position in most of the columns, generating more than 5% of outliers. In the scan, the inner fingerprint is represented as a scattered point cloud, rather than a continuous surface. The clarity and density of the point cloud varies among different subjects, from a very clear almost continuous representation to a complete lack of observable inner fingerprint, which causes the method to generate the largest number of outliers for the inner fingerprint layer.

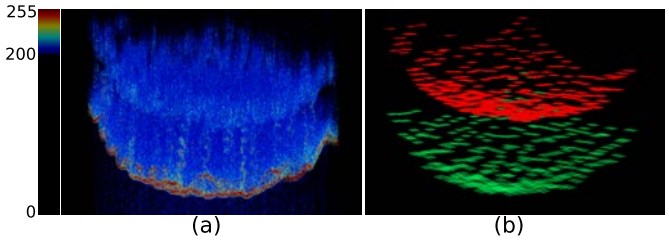

Figure 7: (a) OCT scan of a genuine finger, thresholded (b) Segmentation into 2 layers ($P = 2, l = 36$)

Fig. 8 illustrates detection of 3 layers ($P = 3$) in a fake fingerprint scan.

In addition, an experiment was carried out regarding usability of the overall energy of the layers for artefact detection. The layer detection was run with $P = 3$, in order to detect three layers in an OCT scan. For each layer detected, the energy, e, of the peaks was summed, providing for a vector (S_{e1}, S_{e2}, S_{e3}). The vector was used for classification by

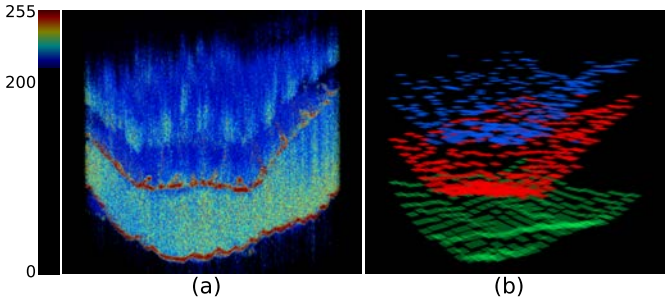

Figure 8: (a) OCT scan of an artefact finger, thresholded (b) Segmentation into 3 layers ($P = 3$, $l = 36$)

means of an SVM classifier with a Gaussian kernel. The Table 1 lists the classification results, cross-validated using 5 different randomly chosen configurations of 50% training and 50% testing data. The results are presented in terms of the ISO/IEC 30107 False Non-Live Detection Rate (FNLDR) and False Live Detection Rate (FLDR) metrics [ISO]. The FNLDR metric represents the proportion of genuine fingerprint scans incorrectly classified as being artefact ones, while the FLDR metric represents the proportion of artefact fingerprint scans incorrectly classified as being genuine. *FLDR train* and *FNLDR train* represent results on the training data, while *FLDR test* and *FNLDR test* demonstrate results on the testing data.

Table 1: Results of the SVM classification using the overall energy of three layers ($P = 3$)

our approach	FLDR train	FNLDR train	FLDR test	FNLDR test
#1	10.99%	3.86%	11.01%	3.36%
#2	11.73%	3.42%	11.37%	3.88%
#3	10.60%	3.75%	12.12%	3.34%
#4	11.45%	3.44%	11.11%	3.55%
#5	11.31%	3.77%	10.97%	3.47%
average performance	11.22%	3.65%	11.32%	3.52%
[Men11]			25.37%	6.17%

5 Conclusions and Future Work

A method for an efficient detection of boundaries between layers in an OCT fingerprint scan has been developed. Our method is able to estimate positions of the boundaries at least two orders of magnitude faster than the method by Menrath and Breithaupt [Men11]. Our classification results demonstrate that even by simply analyzing the energies of the detected layers, our approach outperforms the method by Menrath and Breithaupt [Men11], which confirms robustness of the layer detection method and its potential for further de-

velopment.

Future work would concern further automated analysis of the detected outer an inner fingerprint layers. Development of a new database of OCT fingerprint scans is planned in the framework of the project *OCT-Finger II*. A new OCT scanning technology with better signal to noise ratios, faster acquisition times and higher resolutions[KCGK12] is expected to provide for data that would allow for reliable analysis of fine structures in an OCT scan. It can be attempted to compare the outer and the inner fingerprint structure, since the patterns are identical if the fingerprint OCT scan is genuine. In case of the artefact fingerprints, a falsely detected inner fingerprint layer would yield different fingerprint pattern than the outer layer. Structure and density of the layers could be also analyzed for liveness detection. Genuine fingerprints typically produce the second inner fingerprint layer in a form of a scattered point cloud, in contrast to a rather continuous thin second layer in artefact fingerprint scans. The presence of three distinct layers or only a single layer provide for a strong evidence that the fingerprint is an artefact. In addition, the structure of the inner layer between the first and the second detected layer could be analyzed. In genuine OCT fingerprint scans, this layer has a specific inner structure and typically contains a number of sweat glands. Verification of the appropriate inner structure would reject the artefact fingerprint scans, since their inner structure between the first and the second layer is determined by the properties of the artefact material.

References

[CSF06] S. Chang, S. Sherif, and C. Flueraru. Large area full-field optical coherence tomography. In *Photonics North*, volume 6343, 2006.

[GFAFMD11] J. Galbally, J. Fierrez, F. Alonso-Fernandez, and M. Martinez-Diaz. Evaluation of direct attacks to fingerprint verification systems. *Telecommunication Systems*, 47:243–254, 2011.

[ISO] ISO/IEC WD 30107. Biometrics - Presentation Attack Detection.

[KCGK12] F. Köttig, P. Cimalla, M. Gärtner, and E. Koch. An advanced algorithm for dispersion encoded full range frequency domain optical coherence tomography. *Opt. Express*, 20(22):24925–24948, Oct 2012.

[Men11] M. Menrath. Fingerprint with OCT. Master's thesis, Fern-Uniersität Hagen in Cooperation with Bundesamt für Sicherheit in der Informationstechnik (BSI), 2011.

[Mun12] A. Munde. Biometrics and Security Evaluations. In *International Biometric Performance Conference (IBPC)*, 2012.

[OCT10] OCT-Finger project. Bundesamt für Sicherheit in der Informationstechnik (BSI), Germany, 2010.

[SMB10] M. Sepasian, C. Mares, and W. Balachandran. Vitality detection in fingerprint identification. *WSEAS Trans. Info. Sci. and App.*, 7(4):498–507, April 2010.

[YGD+12] D. Yambay, L. Ghiani, P. Denti, G.L. Marcialis, F. Roli, and S. Schuckers. LivDet 2011 - Fingerprint liveness detection competition 2011. In *5th IAPR International Conference on Biometrics (ICB), 2012* , pages 208–215, 29 2012-april 1 2012.